



Synthesis of a nanocomposite with holocellulose extracted from barley straw and montmorillonite, and optimization of the removal of methylene blue dye using the synthesized adsorbent

Ali Farzi¹ · Milad Soltani¹ · Alireza Ostadrahimi² · Hamid Soleimanzadeh³ · Mehran Namjoufar¹

Received: 11 June 2023 / Accepted: 26 October 2023 / Published online: 24 November 2023
© The Author(s) 2023

Abstract

In this study, holocellulose was extracted from milled barley straw with different mesh sizes using Laccase enzyme. After extraction, a dual composite was made using montmorillonite clay to remove methylene blue dye from synthetic effluent. Results of different analysis methods including scanning electron microscope, Fourier transform infrared spectroscopy, and BET revealed that prepared nanocomposite presented desired specifications, and for smaller mesh sizes, derived holocellulose had higher quality due to high specific surface area. Response surface methodology was employed to reduce the number of experiments for methylene blue adsorption experiments and to achieve an empirical model for prediction of adsorption efficiency at different operating conditions. The effect of different factors including solution temperature, pH, initial dye concentration, and mesh size of milled barley straw on dye adsorption performance by prepared composite was examined. Maximum removal efficiency was obtained about 95% at temperature of 32 °C, pH of 8, initial dye concentration of 4 mg L⁻¹, and mesh size of 70. Also, isotherm studies were performed on experimental data using Langmuir, Freundlich, Temkin, and Dubinin–Radushkevich isotherm models and results revealed that the adsorption process follows Langmuir model with maximum predicted adsorption capacity of 159 mg g⁻¹, which implies monolayer adsorption. Moreover, thermodynamic study revealed that adsorption of methylene blue is endothermic and spontaneous while enthalpy and Gibbs free energy of adsorption are positive and negative, respectively. Finally, adsorption kinetic study determined that the pseudo-second-order kinetics model with correlation coefficient of about 1 best fitted the experimental results which is the characteristic of chemisorption process.

Keywords Barley straw · Adsorption · Holocellulose-Montmorillonite nanocomposite · Methylene blue · Dye removal

Introduction

One of the principal problems of developing countries is contamination of water resources because of the development of associated industries. Toxic and hazardous materials such as polymers, dyes, organic pollutants, and heavy

metals can be detected in wastewater of various industries such as textile, paper, painting, leather, plastics, cosmetics, and food, most of which are carcinogens (Katheresan et al. 2018; Malyan et al. 2019; Monash & Pugazhenthii 2009). About 10–15% of industrial dyes are left untouched in the dyeing process and enter the environment, specifically water resources. Treatment and recovery of municipal and industrial wastewater to prevent environmental contamination and its reuse have become increasingly prominent in recent decades. Different methods have been proposed and used to remove organic dyes from industrial effluents including chemical oxidation, flocculation, photolysis, adsorption, reverse osmosis, etc. (Katheresan et al. 2018; Bhatia et al. 2017). Most of these methods usually are not economic. Meanwhile, adsorption with bio-based adsorbents is growing as a high-performance and low-cost approach (Yagub et al. 2014; Katheresan et al. 2018). Today, various types

✉ Ali Farzi
a-farzi@tabrizu.ac.ir

¹ Faculty of Chemical and Petroleum Engineering, University of Tabriz, Tabriz, Iran

² Nutrition Research Center, Department of Clinical Nutrition, School of Nutrition & Food Sciences, Tabriz University of Medical Sciences, Tabriz, Iran

³ Department of Applied Chemistry, Faculty of Chemistry, University of Tabriz, Tabriz, Iran

of food and agricultural by-products such as barley straw, wheat straw, rice paddy, chitosan, banana peel, sawdust, sugarcane and coconut stalks, and orange peel are used as enzymatic adsorbents to remove contaminants from various water resources (Yagub et al. 2014; Mostafa et al. 2021; Ahmed & Hameed 2018; Akhayere & Kavaz 2021; Hussein et al. 2007; Laribi et al. 2020).

Cellulose is one of the most abundant natural bio-based polymers on earth. Despite its relatively simple chemistry, the physical structure and morphology of cellulose in plants are complex and heterogeneous (Ludueña et al. 2013). Due to easy maintenance, availability, high specific surface area, suitable special mechanical properties, cost-effective production, safer application, biodegradability and renewability, thermal stability, lower energy consumption for production, and many other advantages, it is a very good alternative to petroleum and plastic materials (Dufresne 2013; Phanthong et al. 2018). Hemicellulose fibers have attracted the attention of many researchers in recent years due to their unique qualities. These fibers are available in many forms, such as films and gels and can be mixed with other materials such as polymers to make composites. They are also used in many fields such as bio-nanocomposites, particularly in the automotive and aerospace industries, packaging industry, production of new filters, gas-impermeable films, and hydrogels. (Siqueira et al. 2010; John & Thomas 2008; Lucenius et al. 2019; Chen et al. 2021). Holocellulose nanocrystal fibers by definition are composed of cellulose and partially hemicellulose fibers while lignin and other extractives are removed (Rabemanolontsoa & Saka 2012; Jiang & Hsieh 2015; Chen et al. 2021). Holocellulose extraction is low-cost compared to cellulose extraction because it needs less energy and chemicals consumption and with recyclability property (Yang & Berglund 2020; Laribi et al. 2020). It combines advantages of cellulose and hemicellulose. It has many applications such as preparation of nano-papers (Galland et al. 2015; Park et al. 2017), composite films (Šimkovic et al. 2017; Li et al. 2017b), thermal insulation aerogels for freeze drying (Huang et al. 2020), and printing inks (Chen et al. 2021). Properties, benefits, and applications of holocellulose fibers are completely described by Yang and Berglund (2020). Despite cellulose nanofibers which are hydrophilic, holocellulose nanofibers are amphiphilic which makes them suitable for use in both polar and non-polar environments (Jiang & Hsieh 2015).

Nanocomposite materials have been extensively studied and researched in recent years. They have found many applications in different fields such as water and wastewater treatment (Etemadi et al. 2021; Beyene & Ambaye 2019; Hnamte & Pulikkal 2022; Adeola & Nomngongo 2022), gas storage (Djeridi et al. 2019; Rezayeenik et al. 2022; Srinivasan et al. 2020), catalysts for different chemical reactions (Zinatloo-Ajabshir et al. 2019; Gerasimov 2022; Liu et al.

2022; Stevanović et al. 2022; Cyganowski & Dzimitrowicz 2022), medicine and treatment (Ramezani & Ripin 2023; Qamar 2021; Huang et al. 2022; Nasef et al. 2023), thermal energy storage (Li et al. 2017a, 2023; Haghighi et al. 2020), and environmental remediation (Mohamed 2022; Singh & Ambika 2018; Goci et al. 2023). At least one of the phases of a nanocomposite has one or more dimensions less than 100 nm and nano-scaled particles are distributed within the dominant phase to increase robustness, resistance, electrical conductivity, and magnetic properties (Camargo et al. 2009). To achieve better properties in nanocomposites, the size distribution of nanoparticles and their dispersion within the matrix of the composite should be controlled. Cellulose-based nanofibers are used for reinforcement of composites materials. These fibers provide robustness and rigidity, and their intrinsic properties determine characteristics of composites (Rouquerol et al. 2013; Ardanuy et al. 2015; Kalia et al. 2011). Hosseini et al. (2022) utilized ternary nanocomposite of carboxymethyl cellulose grafted by polyacrylic acid and decorated with graphene oxide for the removal of methylene blue (MB) and showed that the prepared composite has maximum MB adsorption capacity of 138 mg g⁻¹ after 250 min. Moreover, they conducted reusability tests and showed that 90% of nanocomposite capacity remained unchanged after 9 cycles. Munonde et al. (2023) investigated adsorption removal of MB using MnO₂-reduced graphene oxide (rGO) nanocomposite adsorbent synthesized from rGO nanosheets and MnO₂ nanoparticles, assisted by sonication. The adsorption isotherm study showed that Langmuir isotherm model could fit experimental results more accurately with the maximum adsorption capacity of 156 mg g⁻¹. Also, kinetic study revealed that pseudo-second-order model could predict dynamic adsorption results which is the characteristic of chemisorption. They obtained maximum dye removal efficiency of about 98%.

Holocellulose can be extracted from various plant sources. Although wood is the most important source of holocellulose industrial production (Yang & Berglund 2020; Macfarlane et al. 1999), it has received less attention than other uses of wood (Chen et al. 2011a; Yang & Berglund 2021). Production of fibers from agricultural products such as flax, hemp, cotton, and especially agricultural by-products is of particular interest. Agricultural by-products include wheat and barley straw, rice bran, sugarcane stalks, fruit and vegetable pomace, etc. (Reddy & Yang 2005; Wang et al. 2022; Pennells et al. 2020). These non-wood materials contain less lignin than wood (Poletto 2018; Wang et al. 2022), so their decolorization process is less damaging to the fibers. Agricultural by-products are good candidates for use as adsorbents because they are abundant in nature, cheap and effective, and do not require special operations (Chen et al. 2011b; Mostafa et al. 2021; Ungureanu et al. 2023).

Yao et al. (2015) developed extraction of hemicellulose by hot water using sodium hydroxide in order to decrease cellulose degradation and to achieve higher molecular weight of hemicellulose fibers. They utilized response surface method in order to optimize hemicellulose extraction process. Composition and purity of hemicellulose fibers were analyzed by high-performance liquid chromatography, FTIR, and SEM analysis methods and the results revealed that the solid residual silane extract was similar to commercial hemicellulose extract. Laribi et al. (2020) extracted holocellulose and cellulose from wheat straw and converted them to carboxymethyl holocellulose (CMH) and carboxymethyl cellulose (CMC) and studied their physicochemical properties using FTIR, XRD, TGA, and SEM analysis methods. Also, rheological study of the products showed that their aqueous solutions exhibited non-Newtonian thixotropic behavior. Wang et al. (2022) extracted holocellulose nanofibers from apple rhubarb pomaces using peracetic acid delignification and low energy blending. Diameter of extracted fibers ranged from 29.8 to 54 nm which was lower than diameter of obtained holocellulose fibers from wood (62.2 nm).

Kwon et al. (2015) investigated adsorption of lead on holocellulose aerogels synthesized from wood fibers using hydroxide-urea solution. They studied different factors and showed that by increasing equilibrium concentration of lead and pH of the solution, the adsorption rate was increased. Therefore, they concluded that holocellulose aerogels can effectively be used for the removal of heavy metals, specially lead from water and wastewater. Wu et al. (2017) thermally bonded carboxymethyl chitosan-hemicellulose (CMCH) resins and examined them using FTIR, TGA, and SEM. Then, they studied adsorption characteristics of CMCH as adsorbent of metal ions of Cd (II), Ni (II), Cu (II), Hg (II), Mn (VII), and Cr (VI). Different factors affecting adsorption performance such as pH, temperature, contact time, and initial concentration of metal ions were investigated. Their results showed that the ultimate adsorption process follows quasi-second-order kinetic model and the equilibrium isotherm follows Langmuir model. Their experiments revealed that CMCH can significantly be used as a conceivably recyclable and effective adsorbent for the extraction and recovery of heavy metal ions from wastewater. Ahmed and Hameed (2018) utilized abundant wastes of barley straw as precursor to prepare biochar adsorbent through thermal pyrolysis. Pore characteristics, morphology, and attraction extent of the adsorbent toward salicylic acid were identified. The effects of batch adsorption variables, such as initial salicylic acid concentration, contact time, initial pH, and temperature, on biochar adsorption performance were tested. The salicylic acid/biochar system exhibited spontaneous, chemisorption, and endothermic natures. Considering its favorable pore characteristics and high attraction performance, barley straw biochar could be a suitable adsorbent

to eliminate salicylic acid from wastewaters. Santawee et al. (2019) studied adsorption capacity of holocellulose and lignin extracted from coir pith for the removal of trimethylamine (fishy odor). Their results showed that holocellulose extracted from coir pith had higher removal percentage compared to commercial activated carbon. Akhayere et al. (2020) used barley husk waste as a precursor for the synthesis of nano-silica by following a low energy and sustainable method of acid reflux and heat treatment. Nano-silica was then used for the synthesis of magnetic nano-silica (M-NS) by adding magnetic solution of Fe₃O₄ nanoparticles. Magnetic nano-silica particles were observed to have an average diameter of 162 nm and appeared to be hydrophobic, with a large surface area of ~ 120 m² g⁻¹ and was used as an adsorbent for the removal of petroleum contaminants from water. Results showed that with 0.6 g of M-NS, high uptake efficiency of about 85% was achieved. Soldatkin and Yanar (2023) modified barley straw (BS-C) and corn stalks (CS-C) by citric acid for the purpose of dye pollutants removal from aqueous solutions. They used prepared adsorbent materials for the removal of MB and malachite green (MG) from wastewater. They examined effects of different parameters including pH, contact time, dye concentration, and adsorbent dosage on removal efficiency of cationic dyes and achieved maximum removal efficiency of 97% for MB removal with both adsorbents and 95% and 94% for MG removal with BS-C and CS-C adsorbents, respectively.

In recent years, montmorillonite has been used for the removal of different pollutants from wastewaters such as the removal of heavy metals (Alandis et al. 2019; Akpomie & Dawodu 2016; Sen Gupta & Bhattacharyya 2012; Praus et al. 2008; Naz & Chowdhury 2022), adsorption of textile dyes (Husseien et al. 2007; Cottet et al. 2014; Chen et al. 1999; Almeida et al. 2009; Nogueira et al. 2009), and natural and chemical organics (Yamamoto et al. 2017; Burgos et al. 2002). Also, Zhu et al. (2016) and Zango et al. (2022) reviewed different montmorillonite-based adsorbents for the removal of contaminants.

Cottet et al. (2014) studied characteristics of montmorillonite clay modified by iron oxide for the adsorption and removal of MB in aqueous solutions. They reported maximum adsorption capacity of 71.12 mg g⁻¹ at 333 K. Also, their results revealed that the adsorption process was endothermic and non-spontaneous and also pseudo-second-order kinetic model best fitted the experimental results. However, in another study, Almeida et al. (2009) reported that the adsorption of MB on montmorillonite was spontaneous yet endothermic. Their results also showed that maximum adsorption was achieved at pH of 11, temperature of 60 °C and adsorbent concentration of 3 g L⁻¹. Wang et al. (2020) synthesized montmorillonite supported-poly (acrylamide-co-acrylic acid) hydrogel via polymerization and utilized the prepared adsorbent for the removal of MB from aqueous

solutions. They reported maximum dye removal efficiency of about 97% at high concentration (200 mg L⁻¹). Investigation of adsorption kinetics and isotherm revealed that pseudo-second-order kinetic together with Sips isotherm model could predict experimental results with high accuracy.

In this study, firstly barley straw was grinded into different mesh sizes, and holocellulose nanofibers were extracted from the particles. In the next step, montmorillonite nanoparticles were added to nanofibers in order to obtain a bio-nanocomposite for the removal of MB from aqueous solutions. Finally, different factors for the removal of MB, including solution pH, temperature, nanocomposite particle size distribution, and initial dye concentration, were optimized experimentally based on experimental design and response surface methods. To the best of our knowledge, it is the first time that contaminant removal by holocellulose-montmorillonite (HCMM) composite obtained from barley straw has been performed. Due to abundancy of barley straw and montmorillonite, this work can have economic as well as environmental benefits compared to other adsorbents.

Material and methods

Table 1 shows materials used in this study, their purity and manufacturer. Properties and sources of barley straw and montmorillonite clay was described separately at below.

Barley straw, as a native product of East Azerbaijan province in Iran, was used as the source of holocellulose. For this purpose, some barley straw was provided and ground into very fine particles and then meshed with 50, 100, and 150 mesh number sieves. The samples were dried in an oven at 40 °C for 24 h and then were dewaxed by ethanol and filtered. Filtered samples were dried again in an oven (Fan Azma Gostar, Iran) at 70 °C for 2 h. In the next step, 200 g of pure sample were poured in 1000 mL of distilled water and 2 g of Laccase enzyme was used to remove proteins. Filtered and dried sample was poured in 50 mL distilled water and then sonicated with ultrasound device (Elmasonic, Elma, Germany). Then, the pH of

solution was set at 3 by adding hydrochloric acid into the solution and the sample was left at rest in order to precipitate and remove lignin. Finally, holocellulose nanofibers were extracted by filtering the solution and gathering them on a paper. Extracted holocellulose fibers were dried in an oven at 40 °C for 24 h.

The amount of holocellulose available in barely straw was evaluated using the following equation:

$$\text{HC\%} = \frac{m_1}{m_0} \times 100 \quad (1)$$

where HC% is weight percent of holocellulose in barley straw, and m_1 and m_0 are weights of extracted holocellulose and dried barley straw samples, respectively.

Calculation of moisture content of samples was performed using the following equation:

$$W\% = \frac{w_2 - w_3}{w_2 - w_1} \times 100 \quad (2)$$

where $W\%$ is weight percent of moisture, and w_1 , w_2 , and w_3 are crucible weight, total weight of barley straw and crucible before drying, and total weight of dried barley straw and crucible, respectively.

Functional groups of extracted holocellulose were identified using a Fourier transform infrared (FTIR) spectrometer (Bruker Vector 22, Triad Scientific, USA). Complete description and analysis of the recorded spectra are presented in the Results section.

For preparation of HCMM composite, 7 wt% of sodium hydroxide and 24 wt% of urea were dissolved in distilled water, and temperature of the solution was decreased to 0 °C by placing it in an ice bath. Then, 5 wt% of holocellulose and 5 wt% of montmorillonite clay were added to the solution at that temperature. Finally, the prepared composite was placed in a 2 M hydrochloric acid solution and held in it for 24 h. The prepared composite was then washed by distilled water.

Specific surface area of the composite was calculated using BET analysis method which was performed by Quantachrome ChemBET 3000 device (Jiang & Hsieh 2015; Santawee et al. 2019).

Also, a sample of adsorbent was coated with a very thin layer of gold and then SEM images of the sample were taken using TESCAN MIRA3 FEG-SEM (Czech Republic).

Prepared composite was used for the removal of methylene blue (MB) from aqueous solutions. For this purpose, aqueous solutions with different concentrations of MB were prepared. Then, 0.1 g of HCMM composite was emerged in 100 mL of each solution for the adsorption and removal of MB. After 2 h, a sample from each solution was taken and concentration of remained MB in the solution was recorded using a spectrophotometer (Shimadzu, Japan) at maximum wavelength of 665 nm (Melgoza et al. 2009; Mulushewa

Table 1 Chemicals used in different experiments of the study

Component	Company
Ethanol (96%)	Mojallaly (Iran)
Sulfuric acid (72%)	Mojallaly
Acetic acid (98%)	Merck
Nitric acid (65%)	Mojallaly
Sodium hydroxide (99%)	Merck
Montmorillonite	Merck
Methylene blue	Mojallaly
Urea (99%)	Merck

et al. 2021). In order to convert absorbance values to concentrations of MB, a calibration curve was prepared by recording absorbance values of some control samples with known concentrations of MB in the range of 1–5 ppm. Figure 1 shows calibration curve.

The correlation between absorbance and concentration of MB was obtained from the above curve as the following equation:

$$C = 0.161A + 0.008 \tag{3}$$

where A and C (ppm) are absorbance and concentration of MB in aqueous solution, respectively.

Percentage of MB removal, $R\%$, and adsorption capacity of the composite, $q_e(\text{mg g}^{-1})$ were calculated using the following equations:

$$R\% = \frac{C_0 - C_e}{C_0} \times 100 \tag{4}$$

$$q_e = \frac{(C_0 - C_e)V}{m} \tag{5}$$

where V (L), is volume of the solution, m (g) is the mass of adsorbent, and C_0 and C_e (mg L^{-1}) are initial and equilibrium dye concentrations in the solution, respectively (Namjoufar et al. 2021; Senthil Kumar et al. 2014).

Experimental design and modeling using response surface method

The experimental design and response surface methods (RSM) are helpful for reducing the number of required experiments and finding optimum conditions of a process when the desired response is affected by several variables and a theoretical model is hard to obtain. Usually, first- or second-order models with respect to input variables are used for empirical modeling of the response of a process (Eqs. (6) and (7)) (Myers et al. 2016).

$$y = \beta_0 + \sum_{i=1}^k \beta_i x_i + \epsilon \tag{6}$$

$$y = \beta_0 + \sum_{i=1}^k \beta_i x_i + \sum_{i=1}^k \beta_{ii} x_i^2 + \sum_{i=1}^k \sum_{j=2, j>i}^k \beta_{ij} x_i x_j + \epsilon \tag{7}$$

where y is output or response of the process, $x_i, i = 1, 2, \dots, k$ are input or independent variables, and ϵ is model error.

For calculation of unknown constants of the above models, several experiments should be conducted using experimental design method. There are many fractional or full factorial methods that can be used for this purpose. In this work, four input variables (factors) including barley straw mesh size, initial dye concentration in the solution, solution temperature, and solution pH were selected as input variables. One of the best second-order experimental design methods is central composite design (CCD) method (Myers

Fig. 1 Calibration curve of MB at $\lambda_{\text{max}} = 665 \text{ nm}$

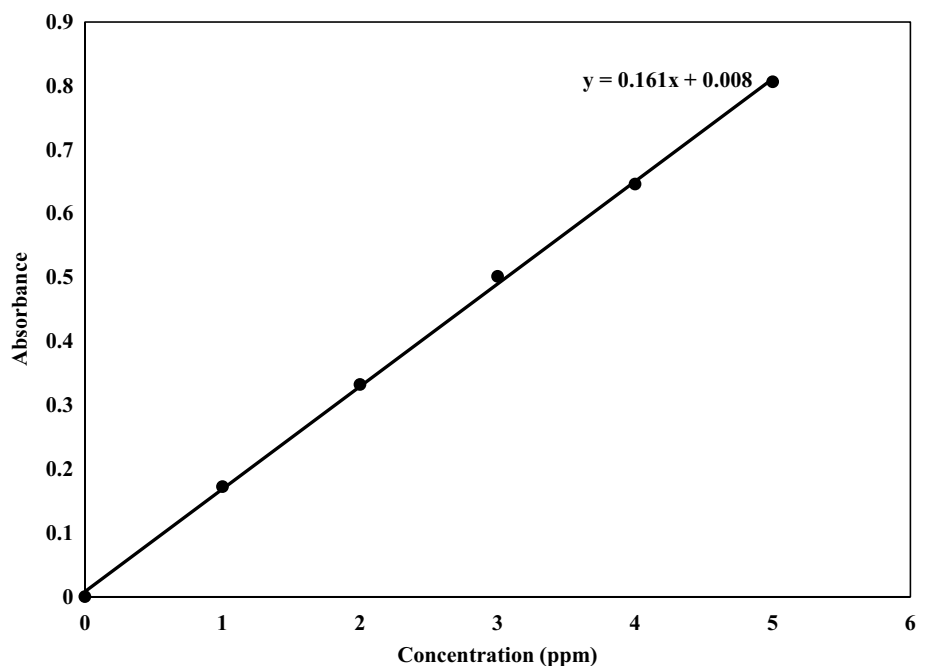


Table 2 Ranges and levels of input variables for experimental design based on CCD method

Factor		Levels			
Complete name	Coded name	Range	-1	0	1
Temperature (°C)	x_1	25–35	25	30	35
pH	x_2	4–8	4	6	8
Initial dye concentration (mg L ⁻¹)	x_3	4–8	4	6	8
Mesh size	x_4	50–150	50	100	150

et al. 2016). For the utilization of CCD method, a matrix of 30 experiments were recommended by Design-Expert software tool (version 10.0.7.1) including 16 factorial points, 8 axial points and 6 repeats of center point of input variables. Table 2 shows ranges of the input variables and their levels. Levels -1, 0, 1 are defined for lower limit, middle value, and higher limit of the factors. Uptake amount of MB by the adsorbent after 120 min of contact time was considered as the response.

Adsorption isotherms

Four adsorption isotherm models including Langmuir, Freundlich, Temkin, and Dubinin–Radushkevich (D–R) were used to identify the equilibrium mechanism of adsorption onto the synthesized composite. Linear forms of these models with respect to their coefficients are presented in the following equations (Namjoufar et al. 2021; Senthil Kumar et al. 2014; Akhayere & Kavaz 2021; Pan et al. 2017; Hu & Zhang 2019; Mousavi et al. 2022b):

$$\frac{C_e}{q_e} = \frac{1}{k_L q_m} + \frac{C_e}{q_m} \quad \text{Langmuir} \quad (8)$$

$$\ln q_e = \ln k_F + \frac{1}{n} \ln C_e \quad \text{Freundlich} \quad (9)$$

$$q_e = B \ln(k_T C_e) \quad \text{Temkin} \quad (10)$$

$$\ln q_e = \ln q_D - k_D \varepsilon^2, \quad \varepsilon = RT \ln \left(\frac{C_s}{C_e} \right) \quad \text{D-R} \quad (11)$$

where C_e (mg L⁻¹) is equilibrium concentration of dye on adsorbent surface in the solution, q_e (mg g⁻¹) is the amount of adsorbed dye at equilibrium, q_m (mg g⁻¹) is maximum adsorption capacity of the adsorbent calculated by Langmuir method, k_L (L mg⁻¹) is Langmuir constant, k_F (mg g⁻¹) is Freundlich constant, n is considered as the heterogeneity of the adsorbent surface, $B = RT/b$ is a constant related to heat of adsorption, k_T (L mg⁻¹) shows equilibrium binding

constant, R (J mol⁻¹ K⁻¹) is the universal gas constant, b is a parameter which is also related to heat of adsorption like B , q_D and k_D are D–R coefficients, and C_s (mg L⁻¹) is solubility of MB in water. Energy of adsorption can be calculated using k_D as (Pan et al. 2017; Togue Kamga 2018):

$$E = \frac{1}{\sqrt{2k_D}} \quad (12)$$

Thermodynamic study

Gibbs free energy of adsorption can be written as follows:

$$\Delta G^{\text{ads}} = -RT \ln K_C \quad (13)$$

where K_C is distribution coefficient of adsorption and is defined as (Chowdhury et al. 2011):

$$K_C = \frac{C_a}{C_e} = \frac{q_e \rho_{\text{ads}}}{C_e} \quad (14)$$

where C_a (mg L⁻¹) is equilibrium concentration of adsorbed material on the adsorbent and ρ_{ads} (kg m⁻³) is adsorbent density. For estimation of heat of adsorption, the Clausius–Clapeyron equation for liquid phase can be applied as follows (Builes et al. 2013):

$$\Delta H^{\text{ads}} = -RT^2 \left(\frac{\partial \ln(C_e)}{\partial T} \right)_{q_e} \quad (15)$$

By applying the above equation on Temkin and D–R isotherm models, Eqs. (16) and (17) can be obtained for the calculation of heat of adsorption, respectively:

$$\Delta H_{\text{Temkin}}^{\text{ads}} = bq_e \quad (16)$$

$$\Delta H_{\text{D-R}}^{\text{ads}} = \Delta H_{\text{fus}} - \varepsilon \quad (17)$$

where ΔH_{fus} is the heat of fusion of MB. Equation (17) is obtained using the following equation (Salimi & Roosta 2019):

$$\frac{1}{x_{\text{MB}} \gamma_{\text{MB}}} = \exp \left(\frac{\Delta H_{\text{fus}}}{RT_t} \left(\frac{T_t}{T} - 1 \right) + \frac{\Delta C_p}{R} \left(\ln \frac{T_t}{T} - \frac{T_t}{T} + 1 \right) \right) \quad (18)$$

where x_{MB} , γ_{MB} , T_t , and ΔC_p are soluble mole fraction of MB, activity coefficient of MB in liquid phase, fusion temperature, and solid–liquid heat capacity difference of MB, respectively. It was assumed that γ_{MB} and ΔH_{fus} are weak functions of temperature and ΔC_p is zero. According to the work of Salimi and Roosta (2019), solubility of MB at 32 °C was estimated as 54.33 g L⁻¹ by linear regression and heat of fusion of MB was set to 26.22 kJ mol⁻¹.

Modeling of the kinetics of dye removal by the composite adsorbent

Kinetics of adsorption process can give valuable information about the rate of adsorption which is necessary for process design and control. In last part of the study, an aqueous solution containing 60 ppm of MB was prepared and kinetic experiments were performed. In certain time periods, a sample from the solution was taken and concentration of MB within the solution was obtained by spectrophotometry and then MB uptake amount was calculated using the following equation (Namjoufar et al. 2021):

$$q_t = \frac{(C_0 - C_t)V}{m} \quad (19)$$

where q_t (mg g⁻¹) is the adsorbed dye uptake amount by the adsorbent, and C_t (mg L⁻¹) is concentration of dye in the solution at time t (min). Obtained experimental data were used for kinetic modeling. In this study, three different models including pseudo-first-order (linear driving force), pseudo-second-order, and intraparticle diffusion models were assessed and their parameters were obtained by fitting experimental data on them. Linear driving force (LDF) model can be written as follows (Naidu & Mathews 2021; Mahmoodi et al. 2012):

$$\frac{dq_t}{dt} = k_1(q_e - q_t) \quad (20)$$

where k_1 (min⁻¹) is the rate constant of the model. This model states that the rate of adsorption is directly proportional to the number of free sites of the adsorbent (Mahmoodi et al. 2012). Integration of the above model and rearranging will result in the following equation (Simonin 2016):

$$\log(q_e - q_t) = \log(q_e) - \frac{k_1 t}{2.303} \quad (21)$$

Therefore, if pseudo-first-order model holds for the provided data, plot of $\log(q_e - q_t)$ with respect to time should give a straight line.

The pseudo-second-order equation can be written as:

$$\frac{dq_t}{dt} = k_2(q_e - q_t)^2 \quad (22)$$

where k_2 (min⁻¹) is the reaction rate constant of pseudo-second-order model (Namjoufar et al. 2021). Integration of the above model with respect to time will give (Pan et al. 2017):

$$\frac{t}{q_t} = \frac{1}{q_e^2 k_2} + \frac{t}{q_e} \quad (23)$$

which means that if this model holds, the diagrams of t/q_t with respect to t should give a straight line (Wang et al. 2016).

Another kinetic model that was used in this study is intraparticle diffusion kinetic model, which can be written as (Mane et al. 2007; Pan et al. 2017; Cheng et al. 2020):

$$q_t = k_3 t^{0.5} + I \quad (24)$$

where k_3 (mg g⁻¹ min^{-0.5}) is intraparticle diffusion rate constant. In order that this model to fit the experimental data, diagram of q_t with respect to $t^{0.5}$ should give a straight line (Pan et al. 2017; Mane et al. 2007). The value of I gives an idea about the thickness of adsorption boundary layer. The larger the intercept, the thicker is the adsorption boundary layer (Mane et al. 2007).

Results and discussion

Results of SEM analysis

SEM images of barley straw, extracted holocellulose, and prepared bio-nanocomposite, are shown in Fig. 2a–c. As can be seen, barley straw nanofibers are in the form of irregular aggregates. After extraction, the form of holocellulose is almost fibrous (Fig. 2b). It is also obvious from Fig. 2c that after preparation of the composite, the particles and aggregates of montmorillonite are distributed almost uniformly between holocellulose fibers. The aggregate particles are in cubic form with a size of about 500–900 nm in at least one dimension which confirms that a nanocomposite material has been synthesized. The difference in contrast of clay nanoparticles and holocellulose fibers is due to the difference in their molecular mass (Goldstein et al. 2018).

BET analysis results

As mentioned before, BET analysis was performed on HCMM composite in order to calculate average particle size, pore volume, and surface area of the adsorbent. According to the results shown in Table 3, high specific surface area was obtained and the composite can be classified as macroporous material due to relatively large average pore size (Somo et al. 2022).

Porosity of composite material can be obtained using the following equation (Hussaini & Dvorkin 2021) assuming homogenous spherical particles:

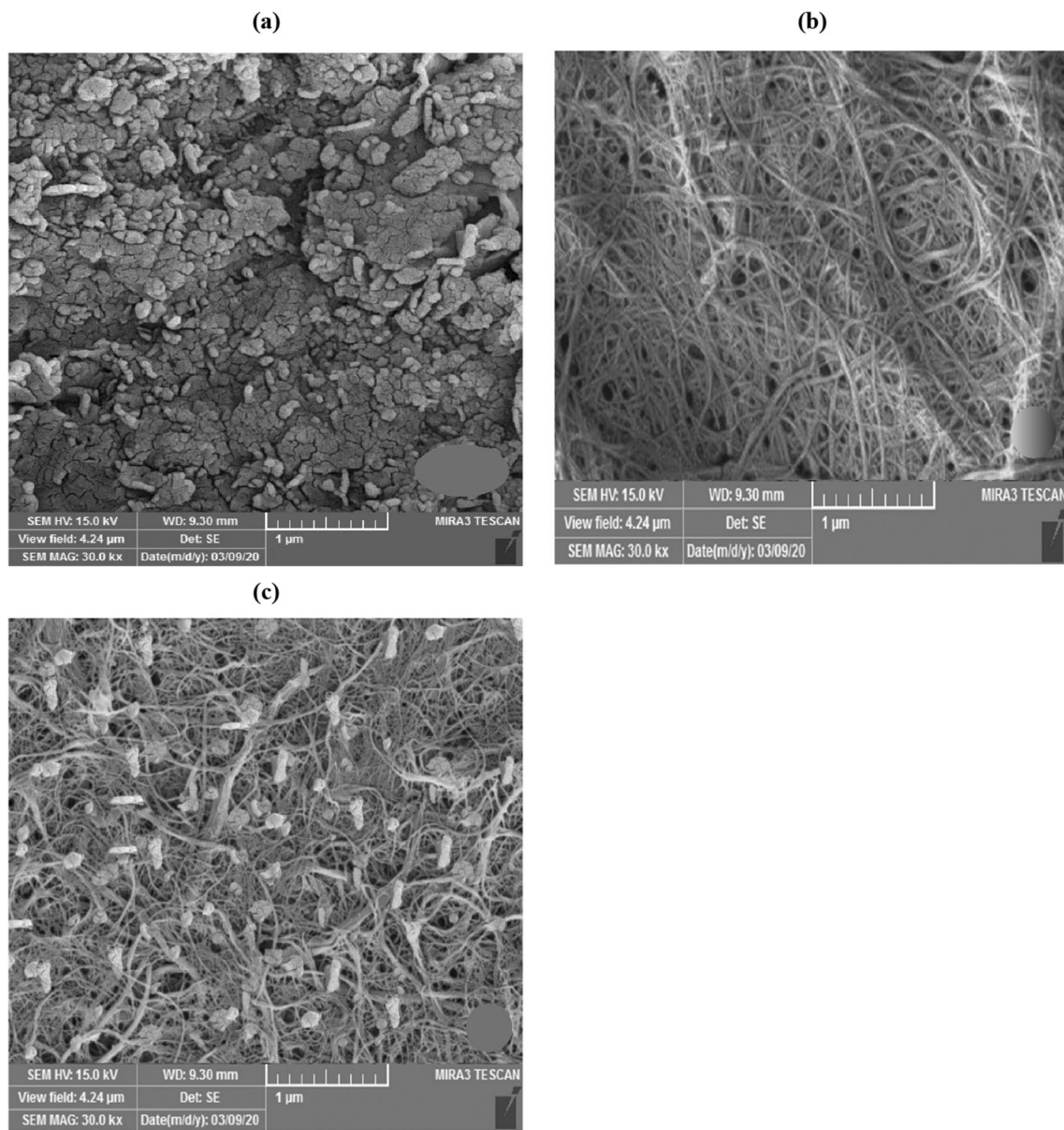


Fig. 2 SEM results: a barley straw, b extracted holocellulose, and c HCMM nanocomposite

Table 3 BET analysis results obtained for HCMM composite

Adsorbent	Specific surface area (m ² g ⁻¹)	Total pore volume (cm ³ g ⁻¹)	Average particle size (nm)
HCMM	25.147	8.635	84.172

$$S = 6 \frac{1 - \phi}{d_p} \tag{25}$$

where S (1/m), d_p (m), and ϕ are specific surface area, average particle size, and porosity of HCMM, respectively. Using the data from Table 3 and assuming that density of

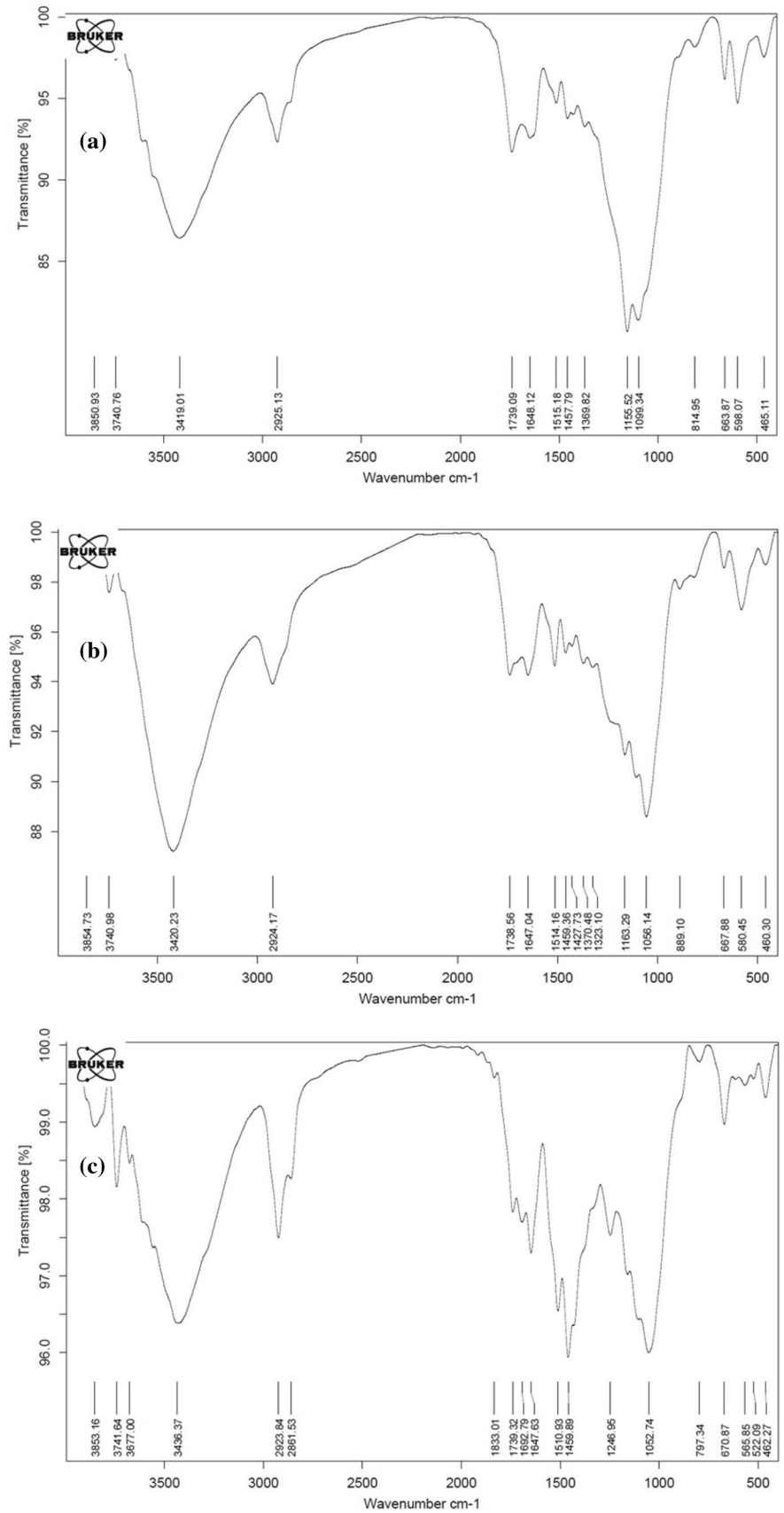
non-porous HCMM is about 900 kg/m³ by neglecting the effect of MM nanoparticles on the density of adsorbent (Sun 2005), porosity of HCMM was obtained about 0.7. Therefore, the density of porous HCMM can be estimated as:

$$\rho_{\text{porous}} = \rho_{\text{non-porous}} \phi \cong 630 \text{ kg/m}^3 \tag{26}$$

Results of FTIR analysis

Results of FTIR analysis of extracted holocellulose for the three mesh sizes of barley straw are shown in Fig. 3a–c. In

Fig. 3 FTIR results. Cellulose synthesized with mesh sizes **a** 50, **b** 100, and **c** 150



the range of 3400–3450 cm^{-1} , wide and strong peaks are seen, which indicate the stretching vibrations of the O–H groups. The presence of these vibrations indicates extraction of cellulose and hemicellulose, due to the existence of many O–H groups in the structure of these compounds. Also, in the range of 2920–2930 cm^{-1} , a relatively strong peak is observed, which is due to the stretching vibrations of the C–H groups in the cellulose structure. Various peaks in the range of 1730–1750 cm^{-1} are evident in all three samples which are related to the vibrations of the C=O group in the hemicellulose structure. A relatively slight peak is also observed in the range of 1640–1650 cm^{-1} , which indicates O–H group related to water adsorption. Fine absorption peaks appear in the range of 1250 to

1450 cm^{-1} which correspond to the symmetric and asymmetric vibrations of C–H groups. Another relatively strong peak in the range of 1050 to 1150 cm^{-1} is related to the C–O group vibrations found in both cellulose and hemicellulose (Atykyan et al. 2020; Galletti et al. 2015). It is worth to note that by decreasing the particle sizes of barley straw (increasing mesh sizes), the intensities of peaks related to O–H and C=O increase sharply. These peaks indicate that extraction of hemicellulose increases with increasing mesh size.

Table 4 Results of experimental runs based on values of factors generated by experimental design

Run	x_1 : T ($^{\circ}\text{C}$)	x_2 : pH	x_3 : MB initial concentration (mg L^{-1})	x_4 : Mesh size	MB removal (%)
1	25	8	4	150	84.90
2	30	6	6	100	89.31
3	30	6	4	100	90.71
4	30	6	6	50	91.09
5	30	6	6	100	89.34
6	25	8	8	50	87.38
7	30	8	6	100	92.12
8	30	4	6	100	87.16
9	35	8	4	50	92.14
10	35	4	8	50	85.56
11	30	6	6	150	85.15
12	35	6	6	100	88.86
13	35	8	4	150	91.16
14	35	8	8	150	87.57
15	25	4	8	150	77.24
16	35	4	4	150	84.04
17	30	6	6	100	89.61
18	35	4	8	150	80.90
19	25	8	8	150	80.34
20	35	4	4	50	87.16
21	25	6	6	100	85.77
22	30	6	6	100	89.31
23	35	8	8	50	90.82
24	25	4	4	50	89.43
25	30	6	8	100	86.87
26	30	6	6	100	89.14
27	25	8	4	50	91.03
28	30	6	6	100	90.14
29	25	4	4	150	81.58
30	25	4	8	50	85.48

Optimization of the removal of methylene blue adsorption by HCMM

Table 4 shows experimental design matrix and also experimental results of MB removal%. As it can be seen, minimum and maximum removal percentages are 77.24 and 92.14.

Based on the experimental results, a second-order model was fitted to find relations between effective factors and the MB removal amount by synthesized adsorbent using linear regression which is presented as the following equation.

$$\begin{aligned} \hat{R}\% = & 43.77 + 3.837x_1 - 2.966x_2 - 0.245x_3 \\ & - 0.0921x_4 - 0.07960x_1^2 \\ & + 0.0838x_2^2 - 0.1288x_3^2 - 0.000474x_4^2 \\ & + 0.08819x_1x_2 + 0.04281x_1x_3 \\ & + 0.004313x_1x_4 - 0.0014x_2x_3 \\ & + 0.004044x_2x_4 - 0.003194x_3x_4 \end{aligned} \tag{27}$$

where \hat{R} is the estimated removal efficiency by the regression model. Results of the analysis of variance of the above

Table 5 Analysis of variance of the obtained model for the response of the amount of adsorbed MB using synthesized bio-nanocomposite adsorbent

Source	DF	Adjusted SS	Adj MS	F value	p value
Model	14	401.025	28.6446	218.33	0.000
x_1	1	6.457	6.4568	49.21	0.000
x_2	1	2.068	2.0680	15.76	0.001
x_3	1	0.014	0.0141	0.11	0.748
x_4	1	2.209	2.2090	16.84	0.001
x_1^2	1	10.260	10.2603	78.20	0.000
x_2^2	1	0.291	0.2908	2.22	0.157
x_3^2	1	0.687	0.6872	5.24	0.037
x_4^2	1	3.638	3.6382	27.73	0.000
x_1x_2	1	12.443	12.4433	94.84	0.000
x_1x_3	1	2.933	2.9327	22.35	0.000
x_1x_4	1	18.598	18.5977	141.75	0.000
x_2x_3	1	0.001	0.0005	0.00	0.951
x_2x_4	1	2.616	2.6163	19.94	0.000
x_3x_4	1	1.632	1.6320	12.44	0.003
Error	15	1.968	0.1312		
Lack-of-fit	10	1.323	0.1323	1.02	0.523
Pure error	5	0.645	0.1291		
Total	29	402.993			
$R^2 = 99.51\%$		Adj $R^2 = 99.06\%$			

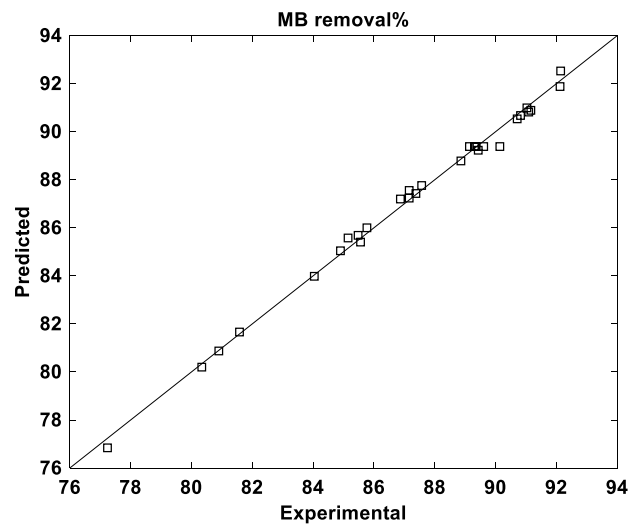


Fig. 4 Comparison of experimental values of MB removal efficiency (%) with predicted values by RSM model

model are shown in Table 5 with 95% confidence level. According to the results, high F value of 218.33, low p value of about zero, and coefficient of determination larger than 99%, designate that the obtained model is statistically acceptable. Regarding significance of different factors, it can be seen from the following table that MB removal% is linearly and quadratically dependent on temperature, and mesh size, and linearly on pH, but does not linearly change with dye initial concentration. Instead, initial concentration affects dye removal efficiency quadratically. Furthermore, according to the following table, binary interactions of all parameters have great effect on dye removal efficiency except for binary interaction of pH and initial concentration which means that these two parameters can be assessed independently of each other.

Figure 4 depicts estimated values of MB removal efficiency calculated by the model compared to the experimental ones which indicates high accuracy of the model for prediction of experimental results within the domains of independent variables.

Effect of pH and temperature on removal efficiency

Figure 5a shows the effect of temperature and pH on MB removal efficiency. As it is evident, the rate of adsorption increases by increasing pH. Maximum adsorption is achieved within temperature range of 30 and 35 °C and pH of 8. Also, at acidic pH values, adsorption amount is decreased. As Österbeg and Claesson (2000) reported, cellulose fibers become compact at acidic pH values and thus available surface for adsorption decreases, while at pH value of 7.3 the fibers swell considerably and thus specific surface area increases. Also, at lower pH values, the composite

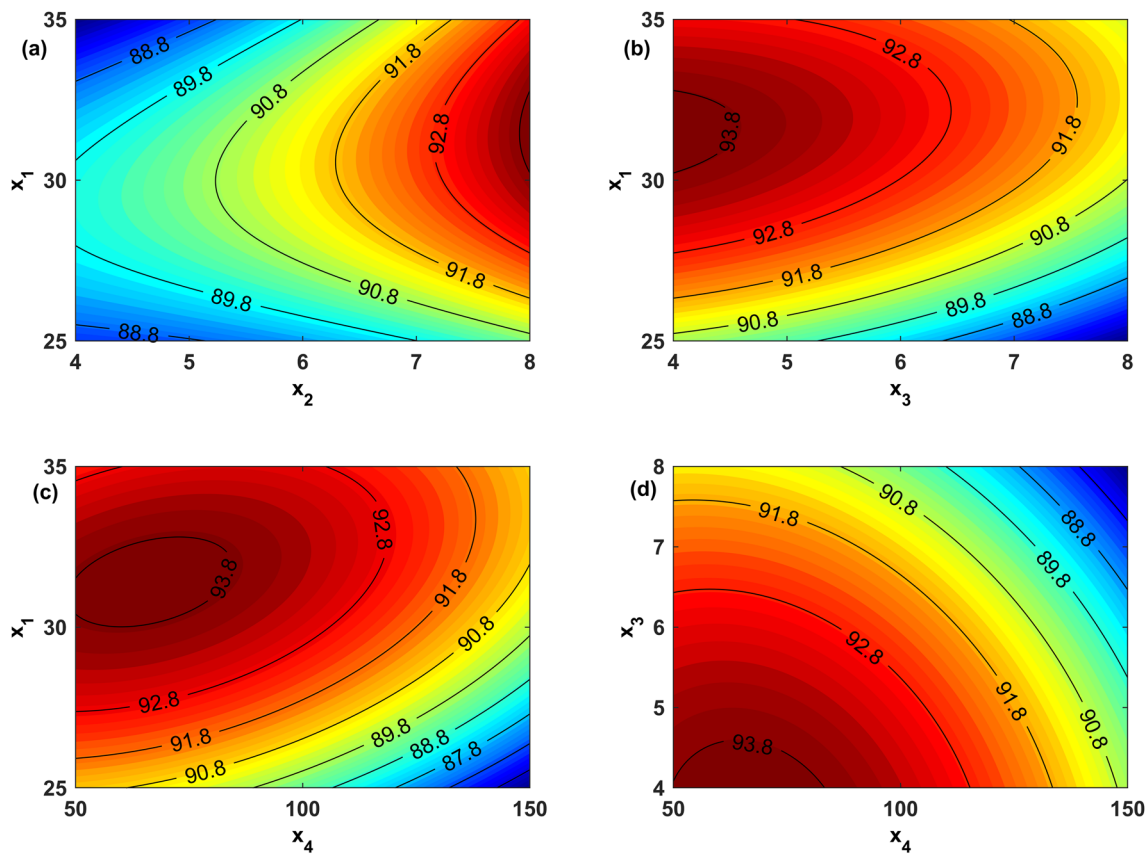


Fig. 5 Contour plot for binary interaction effects on adsorption efficiency of MB using HCMM composite, **a** temperature vs pH, **b** temperature vs. initial dye concentration, **c** temperature vs mesh size, and **d** initial dye concentration vs mesh size

becomes positively charged and while MB is a cationic dye, the repulsion force between dye and composite reduces its adsorption. At alkaline pH values, the composite becomes negatively charged and attracts MB cationic dye, and therefore, by increasing pH, adsorption efficiency increases. For pH values above 9, it has been reported by (Mills et al. 2011) that hydrolysis decomposition of MB takes place and for that reason, experiments were conducted below this critical value.

Effect of temperature and initial MB concentration

Figure 5b illustrates the interactive effect of initial dye concentration and temperature on adsorption efficiency. As can be seen, the extremum point is within temperature range of 30 and 35 °C and initial dye concentration of 4 mg/L. At temperatures lower than 30 °C, the rate of adsorption diminishes because adsorption of MB is

endothermic which will be shown next when presenting results of adsorption isotherms. Also, at temperatures above 35 °C, dye adsorption uptake is reduced which can be deduced to deformation of holocellulose fibers and their thermal expansion. The optimum value for initial concentration of dye is the minimum value tested which is normal while higher concentrations of dye fill active sites of the composite more rapidly and reduce adsorption efficiency. Due to the elliptical nature of the diagram, it can be reasoned that the interaction between these two variables is significant on adsorption efficiency.

Effect of temperature and mesh size on the adsorption rate

Contours and optimum point for these parameters are shown in Fig. 5c. The extremum is at temperature of about 32 °C. In this case, the optimum value for mesh number, which is about 70, is not its lower limit which reflects interactive effect of temperature on this parameter. It could be due to the agglomeration of composite

particles at higher temperatures and lower mesh sizes and reduction of available surface area for adsorption. Also, at higher temperatures, available surface area is decreased due to thermal expansion of fibers and filling of empty spaces. The optimum values of temperature and barley straw mesh size are not located at their assessed lower or higher limits which means that the selected domains for these variables are correct and contain optimum point.

Effect of initial dye concentration and mesh size of barley straw

Figure 5d shows combined effect of initial dye concentration and mesh size of barley straw, used for holocellulose extraction, on the rate of adsorption. As it can be seen, this diagram has a maximum value within the domains

Table 6 Optimum conditions for achieving maximum adsorption efficiency calculated by the aid of RSM model

Variable	Optimum value
Initial concentration of dye (mg L ⁻¹)	4
Temperature (°C)	32
pH	8
Adsorbent mesh size	70
Predicted removal percentage	93.91
Experimental removal percentage at optimal conditions	95.14

of these input variables which means that the assessed parameters have strong interactions with each other. Also, as it was predictable, the maximum adsorption rate was achieved at minimum value of initial concentration of dye, as higher initial dye concentration will decrease adsorption rate due to more rapid filling of active sites of composite. Also, maximum removal efficiency is obtained at smaller values of barley straw mesh size but not its lower limit, because although smaller mesh sizes result in higher amounts of hemicellulose in the extracted holocellulose and higher available surface area for adsorption, but at the same time, much higher specific surface area results in more rapid coating of particles by dye and reduction of removal percentage.

Determination of the optimal conditions

Finally, the optimum point for the independent variables can be calculated using Eq. (27) which is presented in Table 6. The last row of the table is the experimental adsorption value performed at predicted optimum values of independent variables. It is evident that predicted value is very close to the experimental one at optimum point.

Table 7 presents comparison of the adsorption efficiency of MB using HCMM composite obtained in this work with the data gathered from the literature. As it can be seen, the synthesized composite reveals comparable performance with other adsorbents as well as having low cost of synthesis

Table 7 Comparison of adsorption efficiency of MB in this work with other works found in the literature

Adsorbent(s)	Adsorbent dosage (g/L)	Removal percentage	Reference
HCMM	1	77.24–95.14	This work
Activated carbon from <i>Rumex abyssinicus</i> plant	0.2–0.6	82.16–99.96	Fito et al. (2023)
Barley straw and corn stalks modified by citric acid	6–14	48–97	Soldatkina & Yanar (2023)
Activated carbon from Scrap Tire	2.5	89.18–90.48	Kassahun et al. (2022)
Barley Bran and Enset Midrib Leaf	2.5	96–98	Mekuria et al. (2022)
Raspberry (<i>Rubus idaeus</i>) leaves powder	1–5	30–44	Mosoarca et al. (2022)
Activated carbon from grape leaves waste	0.25–12.25	0–97.4	Mousavi et al. (2022a)
Activated carbon from grape wood wastes	0.25–12.25	0–95.66	Mousavi et al. (2022b)
Black tea wastes	13.3	30–72	Ullah et al. (2022)
Carboxymethyl cellulose grafted by polyacrylic acid and decorated with graphene oxide	100	38–97	Hosseini et al. (2022)
Activated carbon from <i>Parthenium hysterophorus</i>	20	86–94	Fito et al. (2020)
Kaolin	1	67–97	Mouni et al. (2018)
Modified sawdust	1.5–5	34.4–96.6	Zou et al. (2013)
Raw and modified mango seed	0.1–1.2	68–99.8	Senthil Kumar et al. (2014)
Montmorillonite modified with iron oxide	0.1	26.78–60.98	Cottet et al. (2014)
Activated carbon from barley straw	0.1	5–70	Husseien et al. (2007)
Fly ash	8–20	45.16–96	Kumar et al. (2005)

Table 8 Predicted values of the parameters of Langmuir, Freundlich, Temkin, and D–R isotherm models for the adsorption of MB dye using HCMM adsorbent

Model	Parameters	
Langmuir	$q_m(\text{mg g}^{-1})$	159
	$k_L(\text{L mg}^{-1})$	0.0956
	R^2	0.984
Freundlich	n	2.52
	$k_F(\text{mg g}^{-1})$	26.42
	R^2	0.891
Temkin	B	29.245
	$k_T(\text{L mg}^{-1})$	1.518
	$b(\text{J g mg}^{-1} \text{mol}^{-1})$	87
	R^2	0.970
Dubinin–Radushkevich	k_D	3.71×10^{-9}
	$q_D(\text{mg g}^{-1})$	420.0
	$E(\text{kJ mol}^{-1})$	11.60
	R^2	0.910

because of using cheap barley straw and montmorillonite clay.

Results of the study of adsorption isotherm models

In order to study the adsorption isotherms related to the synthesized adsorbent and to determine the maximum adsorption capacity of methylene blue, equilibrium data were assessed using Langmuir, Freundlich, Temkin, and Dubinin–Radushkevich (D–R) adsorption isotherm models. The parameters and correlation coefficients of each model are calculated and reported in Table 8. All parameters except initial concentration of dye were set at their optimum values obtained in optimization section. Solutions with different concentrations of dye were prepared and removal of dye by HCMM adsorbent was performed until no changes in dye concentration within aqueous solution were observed. Then, adsorbent material was taken from the solution and was dried in an oven at 90 °C for 24 h. After that, the weight of adsorbent + adsorbed material was measured and the amount of adsorbed material on the adsorbent was calculated according to the initial weight of the adsorbent. Equilibrium uptakes were calculated by dividing adsorbed amount

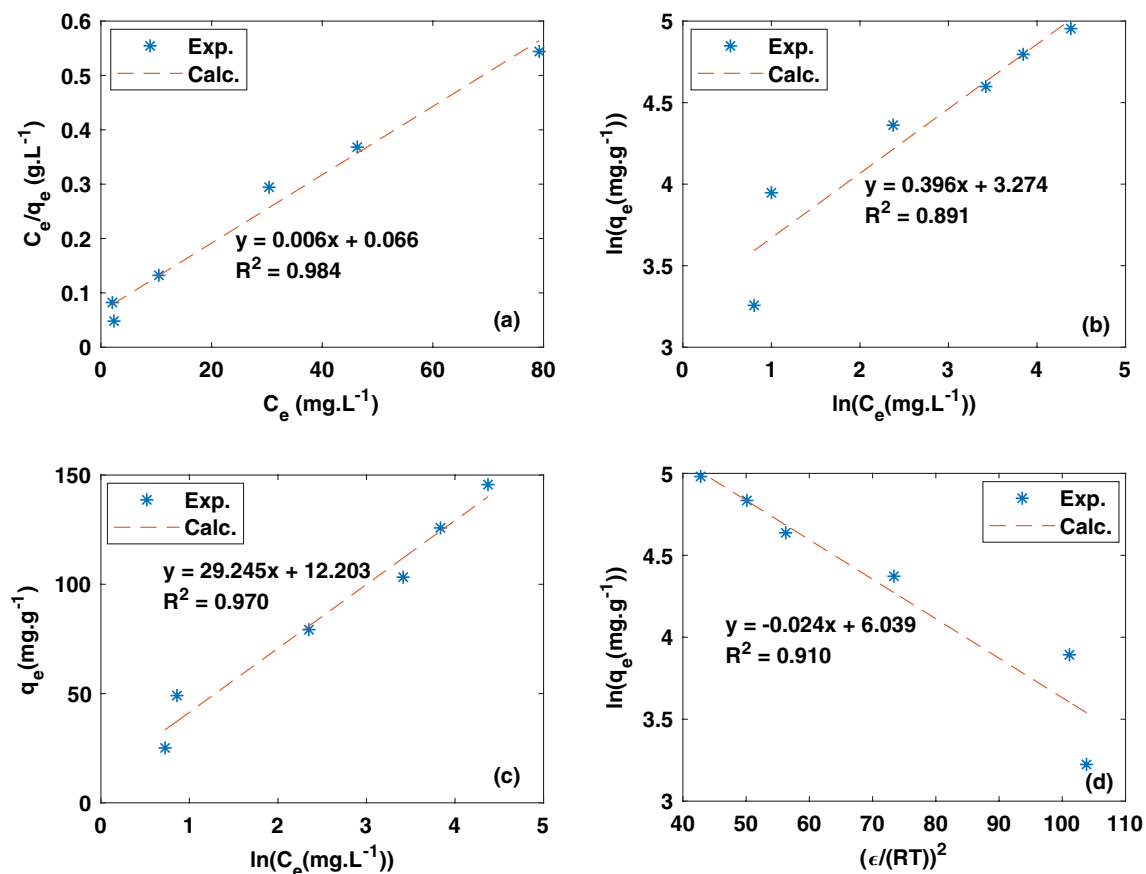


Fig. 6 Linear plots of **a** Langmuir, **b** Freundlich, **c** Temkin, and **d** Dubinin–Radushkevich isotherm models, at 32 °C and pH of 8

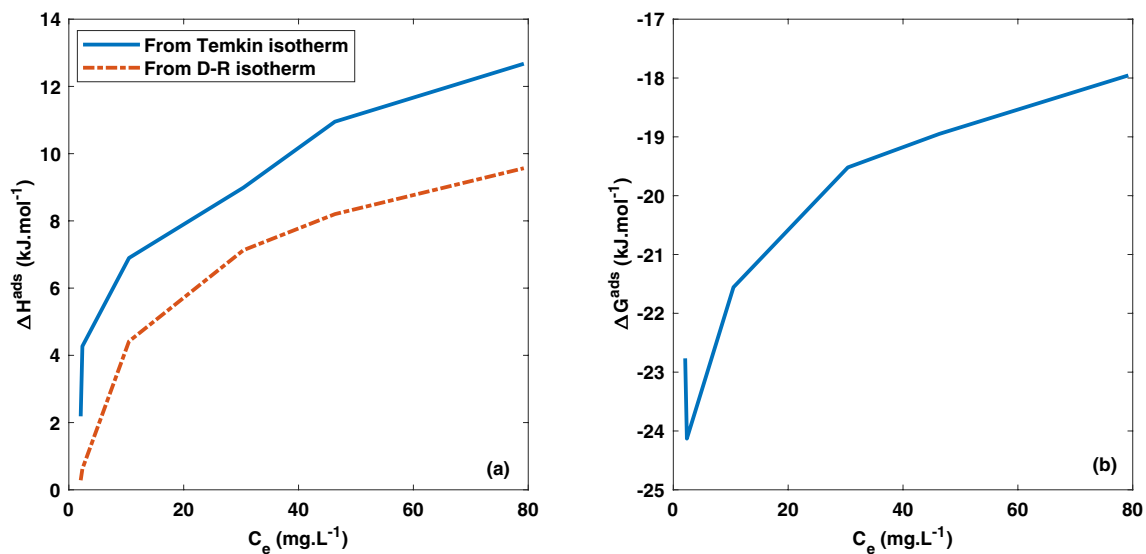


Fig. 7 a Enthalpy of adsorption of MB on HCMM adsorbent at 32 °C and pH of 8 calculated based on Temkin and D–R isotherm models, b Gibbs free energy of adsorption of MB on HCMM adsorbent at 32 °C and pH of 8

onto adsorbent mass. Also, equilibrium concentration of dye in aqueous solution was measured by spectrophotometry according to the method described in Material and Methods section.

Experimental results were applied for finding parameters of isotherm models. Figure 6 (a–d) shows curve fitting of isotherm experimental data at 32 °C and pH of 8 based on Eqs. (8)–(11) which are linear forms of Langmuir, Freundlich, Temkin, and D–R isotherm models in liquid phase, respectively. According to the results, it is evident that Langmuir model with a correlation coefficient of 0.984 fits experimental data more accurately than other isotherm models. Accordingly, it can be concluded that the adsorption of MB happens within homogeneous monolayer surfaces and after adsorption, no interaction exists between adsorbed dye and adjacent adsorbent surface sites (Senthil Kumar et al. 2014; Sahu & Singh 2019). According to Freundlich model, value of n above 1, reveals that adsorption is favorable (Pan et al. 2017). Obtained value for energy of adsorption using D–R isotherm method is 11.6 kJ/mol which indicates chemisorption process (Amin et al. 2015; Pan et al. 2017; Togue Kamga 2018).

Results of thermodynamic study

Figure 7a shows profile of enthalpy of adsorption of MB by HCMM adsorbent at 32 °C which is calculated based on Temkin and D–R isotherm models. It is evident that results with both models are in good agreement with each other and also the adsorption of MB on HCMM is endothermic. Also, Fig. 7b reveals profile of Gibbs free energy of adsorption which is always negative at 32 °C. Therefore, it can be

concluded that the adsorption of MB on HCMM is spontaneous and endothermic. This is a general conclusion for the investigated temperature range in this study, because density of porous HCMM was estimated about $630 \text{ kg}/\text{m}^3$ in BET results section assuming that MM nanoparticles do not have significant effect on the density of adsorbent and therefore heat of fusion of MB and density of composite adsorbent are high enough to make enthalpy of adsorption always positive and Gibbs free energy of adsorption always negative.

Results of kinetic study

According to the results given in Fig. 8a and Table 9, curve fitting by LDF model is not satisfactory while coefficient of determination is low and uptake changes do not have linear relationship with uptake amounts. Also, regarding correlation coefficient of the pseudo-second-order kinetic model given in Table 9 and according to the exact fitting of experimental results shown in Fig. 8b, it can be concluded that this model exactly fits experimental data and offers more satisfactory results. It is well-known that following the pseudo-second-order kinetics is the characteristic of chemisorption process (Agbovi & Wilson 2021) and confirms results of isotherm study. For the intraparticle diffusion model, regarding Fig. 8c, multi-step adsorption is evident. The first step shows adsorption of dye in macropores which is rapid step, while the second step is due to diffusion in micropores (Pan et al. 2017). Also, based on the results of Table 9, intercept of second step of adsorption is higher which indicates higher thickness of microporous adsorption boundary layer and higher resistance against adsorption (Mane et al. 2007).

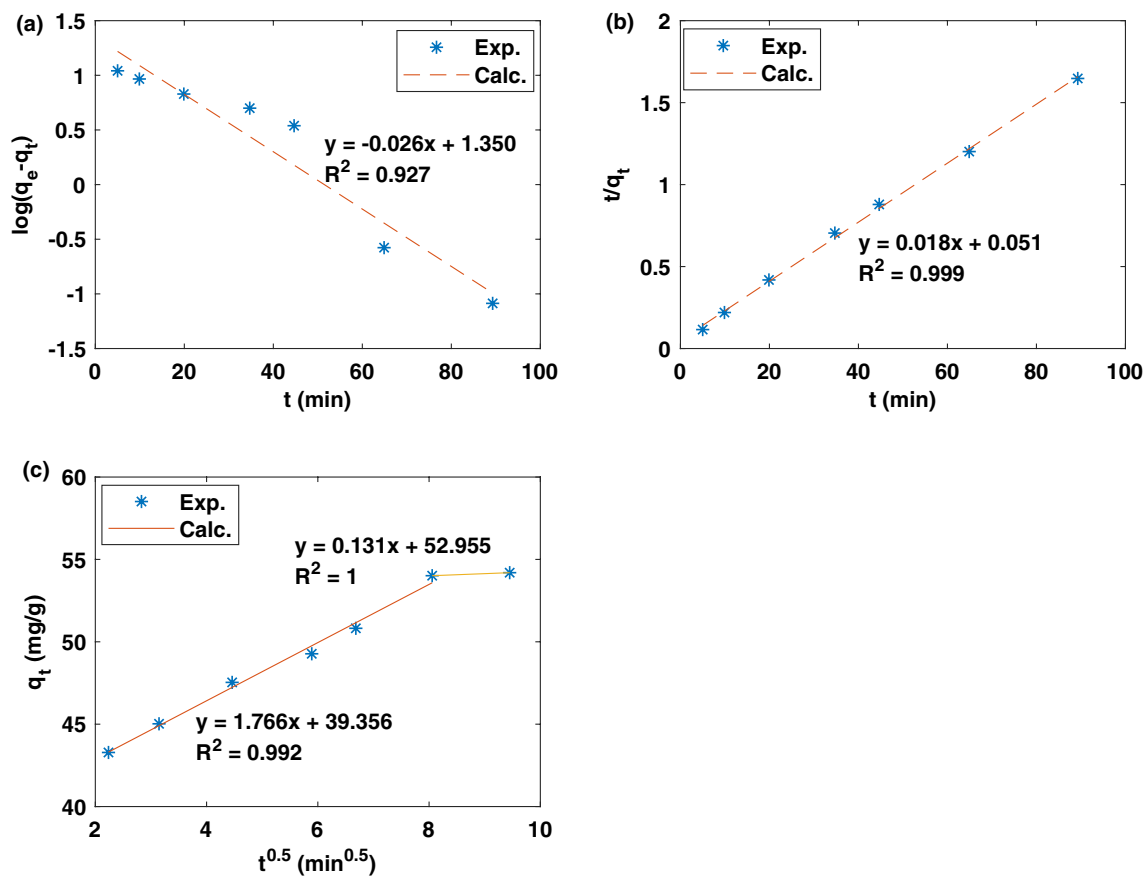


Fig. 8 Linear plots of **a** LDF, **b** pseudo-second-order, and **c** intraparticle kinetic models

Table 9 Calculated parameters of different kinetic models based on experimental data for MB adsorption on HCMM composite

Kinetic model	Parameters	
Linear driving force	$k_1(\text{min}^{-1})$	0.0604
	$q_{e,\text{calc}}(\text{mg g}^{-1})$	22.39
	$q_{e,\text{exp}}(\text{mg g}^{-1})$	54.28
	R^2	0.927
Pseudo-second-order	$q_{e,\text{calc}}(\text{mg g}^{-1})$	55.57
	$k_2(\text{g} \cdot \text{mg}^{-1} \cdot \text{min}^{-1})$	0.018
	R^2	0.999
Intra-particle diffusion	$k_{3,1}(\text{mg g}^{-1} \cdot \text{min}^{-0.5})$	1.766
	$I_1(\text{mg g}^{-1})$	39.36
	R_1^2	0.992
	$k_{3,2}(\text{mg g}^{-1} \cdot \text{min}^{-0.5})$	0.131
	$I_2(\text{mg g}^{-1})$	52.96
	R_2^2	1.000

Conclusions

Removal of environmental pollutants such as dyes from

wastewater is a challenging issue. As literature survey illustrated, adsorption is a promising method for this purpose and utilization of adsorbents based on agricultural wastes has economic and environmental benefits. In this study, holocellulose nanofibers were extracted from milled and powdered barley straw with different mesh sizes. Different analysis methods showed that when a smaller mesh size was used for cellulose extraction, high quality holocellulose was synthesized in terms of its higher effective specific surface area.

After extraction of holocellulose, a nanocomposite was prepared by uniform dispersion of montmorillonite clay nanoparticles on prepared holocellulose. According to the SEM analysis results, the preparation of Holocellulose-Montmorillonite composite was successful because nano-sized clay particles were distributed evenly within holocellulose nanofibers and increased specific surface area of holocellulose. The prepared composite was applied for the removal of methylene blue dye from synthetic aqueous solutions. To find optimal values of the effective operating parameters including solution temperature and pH, initial dye concentration, and mesh size of barley straw powders for the highest removal of methylene blue, response surface methodology was employed. In order to decrease

the number of experiments, experimental design was performed using central composite design method. Based on the experimental results, an empirical second-order model was achieved which was then used to find the optimum values of each parameter. The optimum point was tested again to validate theoretical result of the model. The results revealed that HCMM composite eliminated more than 95% of methylene blue from the solution at optimum conditions. It was shown that by increasing temperature, the adsorption increased and the optimum point was achieved around 32 °C. Also, investigation of the effect of pH showed that the highest adsorptions values were achieved at near neutral to alkaline pH values, i.e., 8. Modeling of the MB adsorption process on HCMM with different isotherm models revealed that it follows Langmuir isotherm model which means that the absorption process is monolayer. Results of thermodynamic study revealed that the process is spontaneous and endothermic and while large values of enthalpy of adsorption were obtained, chemisorption takes place. Finally, kinetic study showed that pseudo-second-order kinetic model best fitted experimental results which also confirms that chemisorption takes place at the surface of the adsorbent and validates results of isotherm and thermodynamic studies.

Acknowledgements The authors acknowledge Department of Clinical Nutrition, School of Nutrition & Food Sciences, Tabriz University of Medical Sciences for providing required facilities for conducting the study. We hereby clarify that the information provided in this paper is true to our belief and knowledge.

Author contributions AF contributed to supervision, literature review, conceptualization, and writing original and final draft of the manuscript. MS contributed to doing experiments, and writing original draft. AO contributed to supervision, methodology, providing facilities and laboratory, and conceptualization. HS contributed to conducting experiments, and advising MS. MN contributed to writing and editing.

Funding The author(s) received no specific funding for this work.

Declarations

Ethical approval Not applicable.

Conflict of interest The authors declare that they have no known competing financial interests or personal relationships that could have appeared to influence the work reported in this paper.

Consent to participate The authors declare their consent to participate in this article.

Consent for publish The authors declare their consent to publish this article.

Open Access This article is licensed under a Creative Commons Attribution 4.0 International License, which permits use, sharing, adaptation, distribution and reproduction in any medium or format, as long as you give appropriate credit to the original author(s) and the source, provide a link to the Creative Commons licence, and indicate if changes

were made. The images or other third party material in this article are included in the article's Creative Commons licence, unless indicated otherwise in a credit line to the material. If material is not included in the article's Creative Commons licence and your intended use is not permitted by statutory regulation or exceeds the permitted use, you will need to obtain permission directly from the copyright holder. To view a copy of this licence, visit <http://creativecommons.org/licenses/by/4.0/>.

References

- Adeola AO, Nomngongo PN (2022) Advanced polymeric nanocomposites for water treatment applications: a holistic perspective. *Polymers* 14(12):2462
- Agbovi HK, Wilson LD (2021) 1 - Adsorption processes in biopolymer systems: fundamentals to practical applications. In: Kalia S (ed) *Natural polymers-based green adsorbents for water treatment*. Elsevier, pp 1–51
- Ahmed MJ, Hameed BH (2018) Adsorption behavior of salicylic acid on biochar as derived from the thermal pyrolysis of barley straws. *J Clean Prod* 195:1162–1169
- Akhayere E, Kavaz D (2021) Nano-silica and nano-zeolite synthesized from barley grass straw for effective removal of gasoline from aqueous solution: a comparative study. *Chem Eng Commun* 208(10):1419–1435
- Akhayere E, Vaseashta A, Kavaz D (2020) Novel magnetic nano silica synthesis using barley husk waste for removing petroleum from polluted water for environmental sustainability. *Sustainability* 12(24):10646
- Akpomie KG, Dawodu FA (2016) Acid-modified montmorillonite for sorption of heavy metals from automobile effluent. *BJBAS* 5(1):1–12
- Alandis NM, Mekhamer W, Aldayel O, Hefne JAA, Alam M (2019) Adsorptive applications of montmorillonite clay for the removal of Ag(I) and Cu(II) from aqueous medium. *J Chem* 2019:7129014
- Almeida CAP, Debacher NA, Downs AJ, Cottet L, Mello CAD (2009) Removal of methylene blue from colored effluents by adsorption on montmorillonite clay. *J Colloid Interface Sci* 332(1):46–53
- Amin MT, Alazba AA, Shafiq M (2015) Adsorptive removal of reactive black 5 from wastewater using bentonite clay: isotherms, kinetics and thermodynamics. *Sustainability* 7(11):15302–15318
- Ardanuy M, Claramunt J, Toledo Filho RD (2015) Cellulosic fiber reinforced cement-based composites: a review of recent research. *Constr Build Mater* 79:115–128
- Atykyan N, Revin V, Shutova V (2020) Raman and FT-IR Spectroscopy investigation the cellulose structural differences from bacteria *Gluconacetobacter sucrofermentans* during the different regimes of cultivation on a molasses media. *AMB Express* 10(1):84
- Beyene HD, Ambaye TG (2019) Application of sustainable nanocomposites for water purification process. In: Inamuddin, Thomas S, Kumar Mishra R, Asiri AM (eds) *Sustainable polymer composites and nanocomposites*. Springer International Publishing, Cham, pp 387–412
- Bhatia D, Sharma NR, Singh J, Kanwar RS (2017) Biological methods for textile dye removal from wastewater: a review. *Crit Rev Environ Sci Technol* 47(19):1836–1876
- Builes S, Sandler SL, Xiong R (2013) Isosteric heats of gas and liquid adsorption. *Langmuir* 29(33):10416–10422
- Burgos WD, Pisutpaisal N, Mazzarese MC, Chorover J (2002) Adsorption of quinoline to kaolinite and montmorillonite. *Environ Eng Sci* 19(2):59–68

- Camargo PHC, Satyanarayana KG, Wypych F (2009) Nanocomposites: synthesis, structure, properties and new application opportunities. *Mater Res* 12:1–39
- Chen G, Pan J, Han B, Yan H (1999) Adsorption of methylene blue on montmorillonite. *J Dispers Sci Technol* 20(4):1179–1187
- Chen W, Yu H, Liu Y, Chen P, Zhang M, Hai Y (2011a) Individualization of cellulose nanofibers from wood using high-intensity ultrasonication combined with chemical pretreatments. *Carbohydr Polym* 83(4):1804–1811
- Chen W, Yu H, Liu Y, Hai Y, Zhang M, Chen P (2011b) Isolation and characterization of cellulose nanofibers from four plant cellulose fibers using a chemical-ultrasonic process. *Cellulose* 18(2):433–442
- Chen Y, Li Y, Liu Y, Chen P, Zhang C, Qi H (2021) Holocellulose nanofibril-assisted intercalation and stabilization of $Ti_3C_2T_x$ MXene inks for multifunctional sensing and EMI shielding applications. *ACS Appl Mater Interfaces* 13(30):36221–36231
- Cheng J, Zhan C, Wu J, Cui Z, Si J, Wang Q, Peng X, Turng L-S (2020) Highly efficient removal of methylene blue dye from an aqueous solution using cellulose acetate nanofibrous membranes modified by polydopamine. *ACS Omega* 5(10):5389–5400
- Chowdhury S, Mishra R, Saha P, Kushwaha P (2011) Adsorption thermodynamics, kinetics and isosteric heat of adsorption of malachite green onto chemically modified rice husk. *Desalination* 265(1):159–168
- Cottet L, Almeida CAP, Naidek N, Viante MF, Lopes MC, Debacher NA (2014) Adsorption characteristics of montmorillonite clay modified with iron oxide with respect to methylene blue in aqueous media. *Appl Clay Sci* 95:25–31
- Cyganowski P, Dzimitrowicz A (2022) Heterogenous nanocomposite catalysts with rhenium nanostructures for the catalytic reduction of 4-nitrophenol. *Sci Rep* 12(1):6228
- Djeridi W, Ben Mansour N, Ouederni A, Llewellyn PL, El Mir L (2019) Elaboration of porous carbon/nickel nanocomposites for selective gas storage. *Solid State Sci* 93:37–43
- Dufresne A (2013) Nanocellulose: a new ageless bionanomaterial. *Mater Today* 16(6):220–227
- Etemadi H, Afsharkia S, Zinatloo-Ajabshir S, Shokri E (2021) Effect of alumina nanoparticles on the antifouling properties of polycarbonate-polyurethane blend ultrafiltration membrane for water treatment. *Polym Eng Sci* 61(9):2364–2375
- Fito J, Abewaa M, Mengistu A, Angassa K, Ambaye AD, Moyo W, Nkambule T (2023) Adsorption of methylene blue from textile industrial wastewater using activated carbon developed from *Rumex abyssinicus* plant. *Sci Rep* 13(1):5427
- Fito J, Abrham S, Angassa K (2020) Adsorption of methylene blue from textile industrial wastewater onto activated carbon of *Parthenium hysterophorus*. *Int J Environ Res* 14(5):501–511
- Galland S, Berthold F, Prakobna K, Berglund LA (2015) Holocellulose nanofibers of high molar mass and small diameter for high-strength nanopaper. *Biomacromol* 16(8):2427–2435
- Galletti A, D'Alessio A, Licursi D, Antonetti C, Valentini G, Galia A, Nasso Di Nasso N (2015) Midinfrared FT-IR as a tool for monitoring herbaceous biomass composition and its conversion to furfural. *J Spectro* 2015:1–12
- Gerasimov E (2022) Synthesis of nanocomposites and catalysis applications. *Nanomaterials (basel, Switzerland)* 12(5):731
- Goci MC, Leudjo Taka A, Martin L, Klink MJ (2023) Chitosan-based polymer nanocomposites for environmental remediation of mercury pollution. *Polymers* 15(3):482
- Goldstein JI, Newbury DE, Michael JR, Ritchie NWM, Scott JHJ, Joy DC (2018) Scanning electron microscopy and x-ray microanalysis. Springer, New York, USA
- Haghighi A, Babapoor A, Azizi M, Javanshir Z, Ghasemzade H (2020) Optimization of the thermal performance of PCM nanocomposites. *J Energy Manag Technol* 4(2):14–19
- Hnamte M, Pulikkal AK (2022) Clay-polymer nanocomposites for water and wastewater treatment: a comprehensive review. *Chemosphere* 307:135869
- Hosseini H, Zirakjou A, McClements DJ, Goodarzi V, Chen W-H (2022) Removal of methylene blue from wastewater using ternary nanocomposite aerogel systems: carboxymethyl cellulose grafted by polyacrylic acid and decorated with graphene oxide. *J Hazard Mater* 421:126752
- Hu Q, Zhang Z (2019) Application of Dubinin–Radushkevich isotherm model at the solid/solution interface: a theoretical analysis. *J Mol Liq* 277:646–648
- Huang H, Yu Y, Qing Y, Zhang X, Cui J, Wang H (2020) Ultralight industrial bamboo residue-derived holocellulose thermal insulation aerogels with hydrophobic and fire resistant properties. *Materials* 13:477
- Huang S, Hong X, Zhao M, Liu N, Liu H, Zhao J, Shao L, Xue W, Zhang H, Zhu P, Guo R (2022) Nanocomposite hydrogels for biomedical applications. *Bioeng Transl Med* 7(3):e10315
- Hussaini SR, Dvorkin J (2021) Specific surface area versus porosity from digital images: high-porosity granular samples. *J Pet Sci Eng* 206:108961
- Hussein M, Amer A, El-Maghraby A, Taha N (2007) Utilization of barley straw as a source of a activated carbon for removal of methylene blue from aqueous solution. *J Appl Sci Res* 3:1352–1358
- Jiang F, Hsieh Y-L (2015) Holocellulose nanocrystals: amphiphilicity, oil/water emulsion, and self-assembly. *Biomacromol* 16(4):1433–1441
- John MJ, Thomas S (2008) Biofibres and biocomposites. *Carbohydr Polym* 71(3):343–364
- Kalia S, Kaith BS, Kaur I (2011) Cellulose fibers: bio-and nano-polymer composites: green chemistry and technology. Springer, Germany
- Kassahun E, Tibebe S, Tadesse Y, Awish N (2022) Synthesis optimization of activated carbon driven from scrap tire for adsorbent yield and methylene blue removal under response surface methodology. *Adv Mater Sci Eng* 2022:2325213
- Katheresan V, Kansedo J, Lau SY (2018) Efficiency of various recent wastewater dye removal methods: A review. *J Environ Chem Eng* 6(4):4676–4697
- Kumar KV, Ramamurthi V, Sivanesan S (2005) Modeling the mechanism involved during the sorption of methylene blue onto fly ash. *J Colloid Interface Sci* 284(1):14–21
- Kwon G-J, Kim D-Y, Kim E-J, Kang J-H (2015) Adsorption capacity of lead on holocellulose aerogels synthesized from an alkali hydroxide—urea solution. *J Korean Phys Soc* 67(4):687–693
- Laribi N, Maatoug S, Jebali Z, Zouari R, Majdoub H, Cheikhrouho M (2020) Low cost carboxymethyl holocellulose and carboxymethyl cellulose from wheat straw. *Cellul Chem Technol* 54(3-4):225–236
- Li X, Zhou Y, Nian H, Zhang X, Dong O, Ren X, Zeng J, Hai C, Shen Y (2017a) Advanced nanocomposite phase change material based on calcium chloride hexahydrate with aluminum oxide nanoparticles for thermal energy storage. *Energy Fuels* 31(6):6560–6567
- Li Z-R, Hu N, Fan L-W (2023) Nanocomposite phase change materials for high-performance thermal energy storage: a critical review. *Energy Storage Mater* 55:727–753
- Li Z, Wang Y, Cheng L, Guo W, Wu G (2017b) Effect of nano- $CaCO_3$ on the structure and properties of holocellulose-fiber/polypropylene biomass composites. *J Wood Chem Technol* 37(1):62–74
- Liu F, Diercks D, Hussain AM, Dale N, Furuya Y, Miura Y, Fukuyama Y, Duan C (2022) Nanocomposite catalyst for

- high-performance and durable intermediate-temperature methane-fueled metal-supported solid oxide fuel cells. *ACS Appl Mater Interfaces* 14(48):53840–53849
- Lucenius J, Valle-Delgado JJ, Parikka K, Österberg M (2019) Understanding hemicellulose-cellulose interactions in cellulose nanofibril-based composites. *J Colloid Interface Sci* 555:104–114
- Ludueña LN, Vecchio A, Stefani PM, Alvarez VA (2013) Extraction of cellulose nanowhiskers from natural fibers and agricultural byproducts. *Fibers Polym* 14(7):1118–1127
- Macfarlane C, Warren CR, White DA, Adams MA (1999) A rapid and simple method for processing wood to crude cellulose for analysis of stable carbon isotopes in tree rings. *Tree Physiol* 19(12):831–835
- Mahmoodi NM, Hayati B, Arami M (2012) Kinetic, equilibrium and thermodynamic studies of ternary system dye removal using a biopolymer. *Ind Crops Prod* 35(1):295–301
- Malyan SK, Singh R, Rawat M, Kumar M, Pugazhendhi A, Kumar A, Kumar V, Kumar SS (2019) An overview of carcinogenic pollutants in groundwater of India. *Biocatal Agric Biotechnol* 21:101288
- Mane VS, Deo Mall I, Chandra Srivastava V (2007) Kinetic and equilibrium isotherm studies for the adsorptive removal of Brilliant Green dye from aqueous solution by rice husk ash. *J Environ Manag* 84(4):390–400
- Mekuria D, Diro A, Melak F, Asere TG (2022) Adsorptive removal of methylene blue dye using biowaste materials: barley bran and enslet midrib leaf. *J Chem* 2022:4849758
- Melgoza D, Hernández-Ramírez A, Peralta-Hernández JM (2009) Comparative efficiencies of the decolourisation of Methylene Blue using Fenton's and photo-Fenton's reactions. *Photochem Photobiol Sci* 8(5):596–599
- Mills A, Hazafy D, Parkinson J, Tuttle T, Hutchings MG (2011) Effect of alkali on methylene blue (C.I. Basic Blue 9) and other thiazine dyes. *Dyes Pigm* 88(2):149–155
- Mohamed RR (2022) Applications of nanocomposites in environmental remediation. In: Shalan AE, Hamdy Makhoul AS, Lanceros-Méndez S (eds) *Advances in nanocomposite materials for environmental and energy harvesting applications*. Springer International Publishing, Cham, pp 453–471
- Monash P, Pugazhenth G (2009) Adsorption of crystal violet dye from aqueous solution using mesoporous materials synthesized at room temperature. *Adsorption* 15(4):390–405
- Mosoarca G, Popa S, Vancea C, Dan M, Boran S (2022) Removal of methylene blue from aqueous solutions using a new natural lignocellulosic adsorbent—Raspberry (*Rubus idaeus*) leaves powder. *Polymers* 14(10):1966
- Mostafa NA, Farouk SM, Abdelhamid SMS, Monazie AM (2021) Optimisation and characterisation of bio-adsorbent based on barley straw and coconut shell. *J Environ Eng Sci* 17(2):89–98
- Mouni L, Belkhir L, Bollinger J-C, Bouzaza A, Assadi A, Tirri A, Dahmoune F, Madani K, Remini H (2018) Removal of Methylene Blue from aqueous solutions by adsorption on Kaolin: kinetic and equilibrium studies. *Appl Clay Sci* 153:38–45
- Mousavi SA, Mahmoudi A, Amiri S, Darvishi P, Noori E (2022a) Methylene blue removal using grape leaves waste: optimization and modeling. *Appl Water Sci* 12(5):112
- Mousavi SA, Shahbazi D, Mahmoudi A, Darvishi P (2022b) Methylene blue removal using prepared activated carbon from grape wood wastes: adsorption process analysis and modeling. *Water Qual Res J* 57(1):1–19
- Mulushewa Z, Dinbore WT, Ayele Y (2021) Removal of methylene blue from textile waste water using kaolin and zeolite-x synthesized from Ethiopian kaolin. *Environ Anal Health Toxicol* 36(1):e2021007
- Munonde TS, Nqombolo A, Hobongwana S, Mpupa A, Nomngongo PN (2023) Removal of methylene blue using MnO₂@rGO nanocomposite from textile wastewater: isotherms, kinetics and thermodynamics studies. *Heliyon* 9(4):e15502
- Myers RH, Montgomery DC, Anderson-Cook C (2016) *Response surface methodology: process and product optimization using designed experiments*. Wiley, USA
- Naidu H, Mathews AP (2021) Linear driving force analysis of adsorption dynamics in stratified fixed-bed adsorbers. *Sep Purif Technol* 257:117955
- Namjoufar M, Farzi A, Karimi A (2021) Removal of Acid Brown 354 from wastewater by aminized cellulose acetate nanofibers: experimental and theoretical study of the effect of different parameters on adsorption efficiency. *Water Sci Technol* 83(7):1649–1661
- Nasef SM, Khozemy EE, Mahmoud GA (2023) pH-responsive chitosan/acrylamide/gold/nanocomposite supported with silver nanoparticles for controlled release of anticancer drug. *Sci Rep* 13:7818
- Naz A, Chowdhury A (2022) Pollutant extraction from water and soil using Montmorillonite clay-polymer composite: a rapid review. *Mater Today: Proc* 60:1–7
- Nogueira FGE, Lopes JH, Silva AC, Gonçalves M, Anastácio AS, Sapag K, Oliveira LCA (2009) Reactive adsorption of methylene blue on montmorillonite via an ESI-MS study. *Appl Clay Sci* 43(2):190–195
- Österberg M, Claesson PM (2000) Interactions between cellulose surfaces: effect of solution pH. *J Adhes Sci Technol* 14(5):603–618
- Pan M, Lin X, Xie J, Huang X (2017) Kinetic, equilibrium and thermodynamic studies for phosphate adsorption on aluminum hydroxide modified palygorskite nano-composites. *RSC Adv* 7(8):4492–4500
- Park C-W, Han S-Y, Choi S-K, Lee S-H (2017) Preparation and properties of holocellulose nanofibrils with different hemicellulose content. *BioResources* 12:6298–6308
- Pennells J, Godwin ID, Amiralian N, Martin DJ (2020) Trends in the production of cellulose nanofibers from non-wood sources. *Cellulose* 27(2):575–593
- Phanthong P, Reubroycharoen P, Hao X, Xu G, Abudula A, Guan G (2018) Nanocellulose: extraction and application. *Carbon Resour Convers* 1(1):32–43
- Poletto M (2018) Lignin—trends and applications. IntechOpen, University of Caxias do Sul, Brazil
- Praus P, Turicová M, Valásková M (2008) Study of silver adsorption on montmorillonite. *J Braz Chem Soc* 19:549–556
- Qamar SUR (2021) Nanocomposites: potential therapeutic agents for the diagnosis and treatment of infectious diseases and cancer. *Colloid Interface Sci Commun* 43:100463
- Rabemanolontsoa H, Saka S (2012) Holocellulose determination in biomass. In: Yao T (ed) *Zero-carbon energy kyoto 2011*. Springer Japan, Tokyo, pp 135–140
- Ramezani M, Ripin ZM (2023) An overview of enhancing the performance of medical implants with nanocomposites. *J Compos Sci* 7(5):199
- Reddy N, Yang Y (2005) Biofibers from agricultural byproducts for industrial applications. *Trends Biotechnol* 23(1):22–27
- Rezayeenik M, Mousavi-Kamazani M, Zinatloo-Ajabshir S (2022) CeVO₄/rGO nanocomposite: facile hydrothermal synthesis, characterization, and electrochemical hydrogen storage. *Appl Phys A* 129(1):47
- Rouquerol J, Rouquerol F, Llewellyn P, Maurin G, Sing KS (2013) *Adsorption by powders and porous solids: principles, methodology and applications*. Academic press
- Sahu O, Singh N (2019) 13 - Significance of bioadsorption process on textile industry wastewater. In: Shahid ul I, Butola BS (eds) *The impact and prospects of green chemistry for textile technology*. Woodhead Publishing, pp 367–416

- Salimi A, Roosta A (2019) Experimental solubility and thermodynamic aspects of methylene blue in different solvents. *Thermochim Acta* 675:134–139
- Santawee N, Treesubsuntorn C, Thiravetyan P (2019) Lignin and holocellulose from coir pith involved in trimethylamine (fishy odor) adsorption. *J Environ Sci* 79:43–53
- Sen Gupta S, Bhattacharyya KG (2012) Adsorption of heavy metals on kaolinite and montmorillonite: a review. *PCCP* 14(19):6698–6723
- Senthil Kumar P, Palaniyappan M, Priyadharshini M, Vignesh AM, Thanjiappan A, Sebastina Anne Fernando P, Tanvir Ahmed R, Srinath R (2014) Adsorption of basic dye onto raw and surface-modified agricultural waste. *Environ Prog Sustain Energy* 33(1):87–98
- Šimkovic I, Kelnar I, Mendichi R, Bertok T, Filip J (2017) Composite films prepared from agricultural by-products. *Carbohydr Polym* 156:77–85
- Simonin J-P (2016) On the comparison of pseudo-first order and pseudo-second order rate laws in the modeling of adsorption kinetics. *Chem Eng J* 300:254–263
- Singh PP, Ambika (2018) 10 - Environmental remediation by nanoadsorbents-based polymer nanocomposite. In: Hussain CM, Mishra AK (eds) *New polymer nanocomposites for environmental remediation*. Elsevier, pp 223–241
- Siqueira G, Bras J, Dufresne A (2010) Cellulosic bionanocomposites: a review of preparation, properties and applications. *Polymers* 2(4):728–765
- Soldatkina L, Yanar M (2023) Optimization of adsorption parameters for removal of cationic dyes on lignocellulosic agricultural waste modified by citric acid: central composite design. *ChemEngineering* 7(1):6
- Somo TR, Hato MJ, Modibane KD (2022) Characterization of macroporous materials. In: Uthaman A, Thomas S, Li T, Maria H (eds) *Advanced functional porous materials: from macro to nano scale lengths*. Springer International Publishing, Cham, pp 87–111
- Srinivasan S, Demirocak DE, Kaushik A, Sharma M, Chaudhary GR, Hickman N, Stefanakos E (2020) Reversible hydrogen storage using nanocomposites. *Appl Sci* 10(13):4618
- Stevanović G, Jović-Jovičić N, Krstić J, Milutinović-Nikolić A, Banković P, Popović A, Ajduković M (2022) Nanocomposite co-catalysts, based on smectite and biowaste-derived carbon, as peroxymonosulfate activators in degradation of tartrazine. *Appl Clay Sci* 230:106718
- Sun C (2005) True density of microcrystalline cellulose. *J Pharm Sci* 94(10):2132–2134
- Togue Kamga F (2018) Modeling adsorption mechanism of paraquat onto Ayous (*Triplochiton scleroxylon*) wood sawdust. *Appl Water Sci* 9(1):1
- Ullah A, Zahoor M, Din WU, Muhammad M, Khan FA, Sohail A, Ullah R, Ali EA, Murthy HCA (2022) Removal of methylene blue from aqueous solution using black tea wastes: used as efficient adsorbent. *Adsorp Sci Technol* 2022:5713077
- Ungureanu EL, Mocanu AL, Stroe CA, Panciu CM, Berca L, Sionel RM, Mustatea G (2023) Agricultural byproducts used as low-cost adsorbents for removal of potentially toxic elements from wastewater: a comprehensive review. *Sustainability* 15(7):5999
- Wang T, Zhao P, Lu N, Chen H, Zhang C, Hou X (2016) Facile fabrication of Fe₃O₄/MIL-101(Cr) for effective removal of acid red 1 and orange G from aqueous solution. *Chem Eng J* 295:403–413
- Wang W, Wang J, Zhao Y, Bai H, Huang M, Zhang T, Song S (2020) High-performance two-dimensional montmorillonite supported-poly(acrylamide-co-acrylic acid) hydrogel for dye removal. *Environ Pollut* 257:113574
- Wang T, Jung J, Zhao Y (2022) Isolation, characterization, and applications of holocellulose nanofibers from apple and rhubarb pomace using eco-friendly approach. *Food Bioprod Process* 136:166–175
- Wu S-P, Dai X-Z, Kan J-R, Shilong F-D, Zhu M-Y (2017) Fabrication of carboxymethyl chitosan–hemicellulose resin for adsorptive removal of heavy metals from wastewater. *Chin Chem Lett* 28(3):625–632
- Yagub MT, Sen TK, Afroze S, Ang HM (2014) Dye and its removal from aqueous solution by adsorption: a review. *Adv Colloid Interface Sci* 209:172–184
- Yamamoto K, Shiono T, Yoshimura R, Matsui Y, Yoneda M (2017) Influence of hydrophilicity on adsorption of caffeine onto montmorillonite. *Adsorp Sci Technol* 36(3-4):967–981
- Yang X, Berglund LA (2020) Structural and ecofriendly holocellulose materials from wood: microscale fibers and nanoscale fibrils. *Adv Mater*, 2001118
- Yang X, Berglund LA (2021) Structural and ecofriendly holocellulose materials from wood: microscale fibers and nanoscale fibrils. *Adv Mater* 33(28):2001118
- Yao S, Nie S, Yuan Y, Wang S, Qin C (2015) Efficient extraction of bagasse hemicelluloses and characterization of solid remainder. *Bioresour Technol* 185:21–27
- Zango ZU, Garba A, Garba ZN, Zango MU, Usman F, Lim J-W (2022) Montmorillonite for adsorption and catalytic elimination of pollutants from wastewater: a state-of-the-arts review. *Sustainability* 14(24):16441
- Zhu R, Chen Q, Zhou Q, Xi Y, Zhu J, He H (2016) Adsorbents based on montmorillonite for contaminant removal from water: a review. *Appl Clay Sci* 123:239–258
- Zinatloo-Ajabshir S, Morassaei MS, Salavati-Niasari M (2019) Eco-friendly synthesis of Nd₂Sn₂O₇-based nanostructure materials using grape juice as green fuel as photocatalyst for the degradation of erythrosine. *Compos B Eng* 167:643–653
- Zou W, Bai H, Gao S, Li K (2013) Characterization of modified sawdust, kinetic and equilibrium study about methylene blue adsorption in batch mode. *Korean J Chem Eng* 30(1):111–122